Journal of Materials Chemistry A

Flow Battery Electroanalysis 3: Online Kinetics Measurements Using Ultramicroelectrodes in Channel Flow

Journal:	*Journal of Materials Chemistry A*
Manuscript ID	TA-ART-03-2022-002132.R1
Article Type:	Paper
Date Submitted by the Author:	17-May-2022
Complete List of Authors:	Segel, Becca; University of Pittsburgh, Chemical and Petroleum Engineering Parr, Zachary; University of Pittsburgh, Chemical and Petroleum Engineering Sawant, Tejal; University of Pittsburgh, Chemical and Petroleum Engineering; Lilac Solutions, Inc. Yim, Carissa; University of Pittsburgh, Chemical and Petroleum Engineering; University of Michigan, Chemical Engineering Miller, Dean; University of Pittsburgh, Chemical and Petroleum Engineering; Stanford University, Chemical Engineering Henry, Thomas; University of Pittsburgh, Chemical and Petroleum Engineering McKone, James; University of Pittsburgh, Chemical and Petroleum Engineering

Journal Name

ARTICLE TYPE

Cite this: DOI: 00.0000/xxxxxxxxxx

Flow Battery Electroanalysis 3: Online Kinetics Measurements Using Ultramicroelectrodes in Channel Flow †

Becca Segel,[a] Zachary Parr[a], Tejal V. Sawant,[a,‡], Carissa S. Yim[a,◇], Dean M. Miller[a,¶], Thomas J. Henry[a] and James R. McKone*[a]

Received Date
Accepted Date

DOI: 00.0000/xxxxxxxxxx

Redox flow batteries are attractive for grid-scale energy storage, but ongoing work on materials discovery is hampered by the difficulty of measuring electron-transfer rates under battery-relevant conditions. We have developed an experimental approach for collecting continuous voltammetric measurements of flow battery electrolytes by placing a 3-electrode cell containing an ultramicroelectrode into the flow loop of a functioning redox flow battery. We further developed an empirical approach for extracting electron-transfer rate constants from each voltammetric cycle, thereby enabling continuous measurements as a function of state of charge and cycle time. Benchmarking these approaches with iron-based aqueous flow battery electrolytes using platinum and carbon fiber ultramicroelectrodes yielded rate constants that varied in the order Pt > electrochemically oxidized carbon > pristine carbon, in good agreement with prior work. We also found that Pt electrodes become more catalytically active upon cycling for several hours, whereas carbon fiber electrodes with and without oxidative pretreatments remained stable over the same interval. We expect these experimental approaches can be used to measure kinetics and other figures of merit for most electrodes and electrolytes of interest for redox flow batteries as well as in other systems where it is useful to evaluate the properties of a flowing electrolyte in real time.

[a] *University of Pittsburgh Department of Chemical and Petroleum Engineering, 3700 O'Hara St, Pittsburgh, PA, 15213. Tel: 412 383 7407; E-mail: jmckone@pitt.edu*

‡ *Present address: Lilac Solutions, Inc. 1700 20th St Oakland, CA 94607. Tel: 40 1714 7906*

◇ *Present address: University of Michigan Chemical Engineering Department, 2300 Hayward St, Ann Arbor, MI 48109. Tel: 73 4764 2383*

¶*Present address: Stanford University Chemical Engineering Department, 443 Via Ortega, Stanford, CA 94305. Tel: 65 0723 4906*

† Electronic Supplementary Information (ESI) available: PDF further describing the experimental set-up and data analysis and PPTX file containing animations that illustrate the shrinking overpotential method.

Introduction

Stationary batteries are valuable for increasing the efficiency and flexibility of the electric grid by storing excess power during periods of low demand and delivering power when the demand is high.[1–3] This type of load leveling will become increasingly important as the proportion of power provided from intermittent renewables continues to grow.[4,5] Due in large part to recent advances in the manufacturing of Li-ion batteries for transportation applications, Li-ion technologies are also the primary focus in the growing market for grid-scale energy storage.[6,7] However, the redox flow battery (RFB) presents an attractive alternative to Li-ion and related battery technologies because the cost per unit of stored energy decreases dramatically as the size of the battery increases.[8–10] This is a direct consequence of the characteristic decoupling in RFBs between the design of redox-active liquid or semisolid electrolytes (and their storage containers) and the charge–discharge stack.

Flow batteries have been under active development for half a century. Early work by NASA in the 1970s focused on transition metal complexes in water, culminating in the development of an iron-chromium RFB.[11,12] The all-vanadium RFB (VRFB) was demonstrated thereafter by Skyllas-Kazacos in 1985, and this remains the most technologically mature RFB chemistry.[13–17] Key advantages for VRFBs include a cell voltage that closely matches the thermodynamic stability window of water and immunity to permanent capacity fade since the vanadium-based positive and negative redox couples are interconvertible and easy to regenerate. However, vanadium ore is costly to recover and process, which limits the ability of VRFBs to meet the anticipated global demand for grid storage.[6,18] Specifically, several techno-economic studies have concluded that redox couples for aqueous RFBs should be at least 2-3 times less costly than vanadium, whereas higher costs are tractable for nonaqueous chemistries with larger cell voltages.[8,12,19]

The need for new RFB chemistries that outperform the incumbent VRFB technology has motivated a surge of research on materials discovery over the past several years. Significant advances from the last decade include aqueous organic redox couples that are stable when cycled in water,[20–23] high voltage nonaqueous electrolytes,[9,24–29] molecules exhibiting multi-electron transfer reactions,[30–35] and unconventional electrolytes based on deep eutectic solvents.[36–38] We encourage readers to consult the available review literature for more comprehensive summaries of ongoing work.[39–41]

A key advantage for redox flow batteries is their ability to operate at high areal current densities.[19] Accordingly, efficient operation requires fast electron-transfer kinetics, and the effective interfacial electron transfer rate constant (k^0_{eff}) is a key figure of merit. Note that we use "effective" here to denote empirically derived rate constants based on superficial electrode areas, which do not consider the areal density and heterogeneity of sites at which electron-transfer occurs. Thus, k^0_{eff} is closely related to the superficial exchange current density J_0 except that it is directly comparable across electrolytes at different concentrations.[42]

Numerous analytical methods have been used to study the electron-transfer kinetics on RFB electrodes and electrolytes.[43–46] The most prevalent approaches include stationary and rotating disk electrode voltammetry,[47–51] electrochemical impedance spectroscopy,[52–56] micropolarization,[57–61] and microelectrode voltammetry.[62–64] Although each of these approaches is based on a firm foundation in analytical electrochemistry,[65] there exist major discrepancies in the reported values of electron transfer rate constants even for the most heavily studied RFB electrodes and redox couples (Figure 1).[66–80] This high level of variability frames an important scientific question: is it possible to accurately measure k^0_{eff} for RFB active materials?

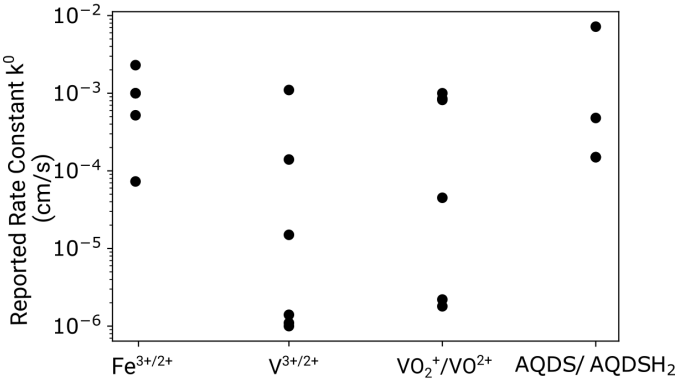

Fig. 1 Compiled rate constant values reported in the existing research literature for carbon electrodes and several widely studied RFB redox couples. Note that AQDS/AQDSH$_2$ refers to the oxidized and reduced forms of anthraquinone disulfonic acid. Tabulated values and references are compiled in the Electronic Supplementary Information.

For the past several years, a major research focus of our lab has been addressing the question above by developing straightforward, replicable methods for measuring electron transfer kinetics in RFBs. Using aqueous $Fe^{3+/2+}$ redox couples as model RFB electrolytes, we first showed that it is possible to obtain reproducible kinetics measurements on noble metals using stationary and rotating disk electrode (RDE) voltammetry, but only if the electrode surfaces are kept scrupulously clean.[81] We also studied $Fe^{3+/2+}$ kinetics at glassy carbon electrodes and found that these are less sensitive to fouling but highly sensitive to electrode pre-treatment conditions.[82] Specifically, we found that oxidative pretreatments markedly improve electron-transfer kinetics for Fe-based RFB electrolytes, but only if they increase the fraction of carbonyl functionalities (as opposed to alcohol or ether functionalities) on the electrode surface.

In the course of our prior studies of RFB kinetics, we also encountered several practical drawbacks for the use of stationary and hydrodynamic voltammetry at macroelectrodes. For example, the relatively large currents (10 mA or more at mm-scale electrodes) that are generated in concentrated (1 M or greater) electrolytes makes it difficult to fully correct for voltage errors due to series resistance, because errors of only a few percent in the measured resistance can have a large impact on the final results. These analytical techniques are also tedious because they require the completion of multiple experiments to extract a single rate constant. This in turn makes it difficult to collect replicate measurements or extend kinetic analysis to multiple states of charge, particularly when electron-transfer rates are sensitive to the history of the electrode surface. Finally, most voltammetric techniques require explicit measurements of transport-limited current densities so that transport contributions can be eliminated mathematically for kinetic analysis. This is a particular problem for RFB studies because the best RFB electrolytes feature redox couples whose reduction potentials are very near the stability limits of the solvent, supporting electrolyte, or electrode. Thus, applying overpotentials that are extreme enough to achieve a transport limit risks irreversible damage to these key battery components. Indeed, practical battery operation usually entails the use of voltage cutoff limits specifically to avoid extended operation under transport-limited conditions.

In this paper, we describe an approach for kinetics measurements that overcomes several of the aforementioned challenges when used with flow battery active materials. We constructed a 3-electrode cell featuring an ultramicroelectrode (UME) in a channel-flow configuration, inserted it into the flow loop of a fully functional RFB, and then used it to execute voltammetry measurements as the battery underwent charge and discharge. We further developed an empirical approach that we call the *shrinking overpotential method* to extract an estimate of k^0_{eff} from each voltammogram. Benchmarking our method using simulated voltammetric data showed that accurate measurements can be made over the full range of state of charge (SOC) values that are relevant for RFB operation and for k^0_{eff} values ranging over several orders of magnitude. We then implemented these tools to measure k^0_{eff} for the $Fe^{3+/2+}$ redox couple at Pt and carbon fiber UMEs. The results broadly agree with prior findings that reaction rates vary in the order Pt > electrochemically oxidized C > pristine C.[68,70,82] Our data also suggest that Pt electrodes are activated by cycling in Fe RFB electrolyte over at least several hours, whereas pristine and oxidized C fiber electrodes remain quite stable on the same timescale.

Experimental Methods

Figure 2 schematizes the apparatus that was used to execute experimental measurements, comprising continuous ultramicroelectrode (UME) voltammetry at platinum and carbon fiber UMEs while cycling an $Fe^{3+/2+}$(aq) electrolyte through various states of charge in a coupled RFB. The Electronic Supplementary Information includes a detailed discussion of experimental methods, and an abbreviated summary is as follows.

The flow battery itself comprised a 10 cm^2 commercial flow battery stack with two 10 mL reservoirs and a peristaltic pump flowing electrolyte at 10 mL/min. The electrodes in the stack were carbon felt and the membrane was Nafion. It was assembled in an unbalanced, compositionally symmetric cell configuration, as described in detail by Goulet and Aziz.[83] The primary advantage of this approach is that it greatly decreases the impact of crossover, as both sides of the cell contain the same electrolyte (albeit at different states of charge). The capacity limiting side of the battery was charged with 3.5 ± 0.5 mL of 1M $FeCl_2$ in 2 M HCl(aq) for kinetics measurements. The non-capacity limiting side was charged with 12.5 mL (which is greater than the reservoir volume because it includes the internal volume of the RFB stack and tubing) of an electrolyte containing 0.5 M each of $FeCl_2$ and $FeCl_3$ in 2 M HCl (aq). The battery was cycled continuously at ±20 mA/cm^2 (normalized by the superficial area of the battery electrodes) over a cell potential of ±0.6 V. This corresponds to a C-rate of ∼2.1C based on the theoretical capacity of the capacity limiting side of the battery.

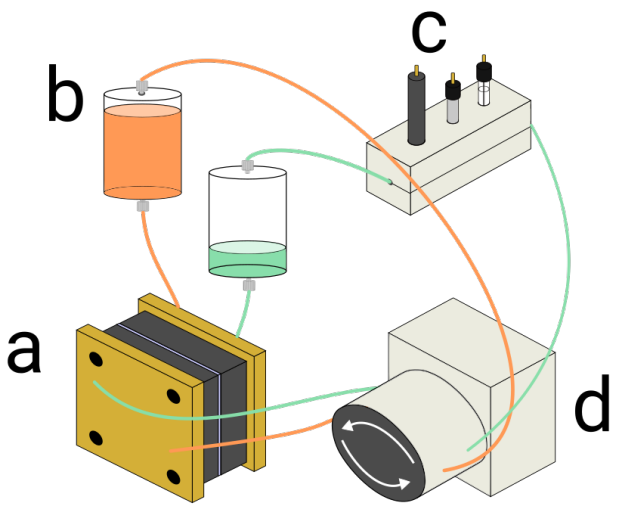

Fig. 2 Schematic representation of the experimental apparatus: (a) RFB cell, which allows for the charge and discharge of the $Fe^{3+/2+}$ electrolyte; (b) electrolyte storage reservoirs, which are gas tight and also function as pulsation dampeners; (c) analytical half cell containing an ultramicroelectrode working electrode, a graphite rod counter electrode, and an Ag/AgCl reference electrode; (d) peristaltic pump that drives fluid flow through the path defined by the tubing demarcated in orange and teal in a counter-clockwise fashion.

A second, home-built electrochemical cell, hereafter referred to as the analytical cell, was placed in fluidic series between the capacity limiting battery reservoir and the peristaltic pump. It contained a 1 x 1 x 35 mm flow channel with threaded holes oriented perpendicular to the flow direction into which commercial working, counter, and reference electrodes were inserted. The working electrodes were either platinum or carbon fiber UMEs; the reference electrode was Ag/AgCl; and the counter electrode was a graphite rod. The working electrodes were prepared by abrasive polishing and additional pre-treatment steps as described previously and further discussed in the Electronic Supplementary Information.[81,82] Cyclic voltammetry measurements were collected continuously by cycling the potential between 0.1 and 0.9 V vs. Ag/AgCl at a scan rate of 20 mV/s.

A single experimental run involved 5 charge–discharge cycles in the RFB and continuous voltammetric cycling as described above. Note that we define the "charging" direction of the battery to be oxidation of the capacity limiting $FeCl_2$ electrolyte, consistent with the use of $Fe^{3+/2+}$ as the positive redox couple in an Fe/Cr RFB. A set of 15 runs were completed in total—5 replicates each of 3 different UME working electrodes. We also completed one longer set of continuous cycling measurements, lasting ∼50 hours, to confirm the general performance and operational stability of the RFB; note that 4.5 mL of capacity limiting electrolyte was used in this case.

We extracted performance metrics—including full cell voltage as well as capacity and coulombic efficiency of the capacity limiting side—–from the RFB cycling data. We also extracted SOC and k^0_{eff} from cyclic voltammetry data, as described in the corresponding sections below. Error bounds are reported as 95 % confidence intervals unless otherwise noted.

Results and Discussion

Battery Behavior

Figure 3 depicts representative charge–discharge data for the RFB cell. Panel 3a shows cell voltage vs. time for one experimental run comprising 5 charge–discharge cycles at 20 mA/cm^2. These data are nearly symmetric about 0 V, which is consistent with the cell configuration in which the composition of the capacity limiting electrolyte varies from predominantly Fe^{3+} to predominantly Fe^{2+}, while the non-capacity limiting side remains very near to equimolar $Fe^{3+/2+}$ throughout the experiment. Panel 3a also depicts the average cell voltages during the charge and discharge cycles, which were 0.20V and −0.16V, respectively. These values enable a rough estimate of the average overpotentials as ≤100 mV each at the anode and cathode. These overpotentials are reasonable given the modest superficial current density and the large electro-active surface areas of the untreated carbon felt electrodes (which were not pre-treated to improve their catalytic properties). We observed distinct "breaking in" behavior in 6 out of 15 RFB charge–discharge experiments, where stable potential vs. time behavior was only achieved after one or several cycles (complete datasets are included in the Electronic Supplementary Information). We attribute this mainly to the time required for the electrolyte to fully wet the electrodes.

Panels 3b and 3c compile capacity and coulombic efficiency

data during 50 cycles of extended charge–discharge. The average capacity during charge was 341 ±2 C and the average capacity during discharge was 339 C ±2 C. This is ∼80% of the theoretical capacity, 434 C, based on the concentration and volume of the capacity limiting electrolyte, which further implies that the capacity limiting side cycled between 10 and 90 % state of charge. The temporal evolution of battery capacity included an initial breaking-in period during which capacity decreased by 20 C over the first 4 cycles. This was followed by approximately 25 more stable cycles with discharge capacities in the range from 337 C to 345 C and coulombic efficiencies exceeding 99 %. Cycles 30–50 then again become somewhat more erratic in capacity and coulombic efficiency. We speculate that the main reason for this behavior in the later cycles was the tendency for small droplets of electrolyte to stochastically attach and detach from the sidewalls of the reservoirs, resulting in small increases and decreases in the volume of the electrolyte available to the RFB cell. Similar behavior was observed and discussed previously by Goulet and Aziz.[83]

These data broadly indicate that the RFB cell stably cycles Fe-based electrolytes over technologically relevant states of charge for at least several hours. This was true even while executing analytical measurements at a second cell in the electrolyte flow loop (see Electronic Supplementary Information, Figure S1). The use of UMEs in the analytical cell is advantageous because the very small associated current flow minimally perturbs the composition of the electrolyte. Note, however, that this system also benefits from the chemical stability of $FeCl_2$ and $FeCl_3$, which allowed us to create electrolytes of arbitrary initial composition by mixing salts on the benchtop. Adoption of this approach for materials where only one half of the redox couple is available would require an additional pre-electrolysis step to generate a symmetric configuration. This type of processes is well-documented for preparation and regeneration of positive and negative electrolytes for VRFBs from a single precursor.[84,85] The $Fe^{3+/2+}$ redox couple is also only weakly air sensitive, where Fe^{2+} slowly oxidizes in the presence of atmospheric oxygen, which further benefits stable cycling. Similar studies using air-sensitive reagents like $V^{3+/2+}$(aq) would require additional efforts to exclude atmospheric oxygen.[86]

Data from the Analytical Cell

Figure 4 collects representative results from UME voltammetry in the analytical cell. The current density vs. potential data in Panel 4a were extracted from a Pt UME during continuous cycling over the time period corresponding to a single charging cycle in the RFB. Hence, the data show clear progression of decreasing anodic current density and increasing cathodic current density as the concentration of Fe^{3+} increases. Notably, the difference between the maximum and minimum current densities (normalized to the superficial area of the UME, 5.9 x 10^{-7} cm^2) approaches 1.5 A/cm^2, which attests to the ability of the UME electrode geometry to achieve very high rates of mass transfer, which are further enhanced by convection in a flowing electrolyte.

We also recorded the temporal progression of the open-circuit

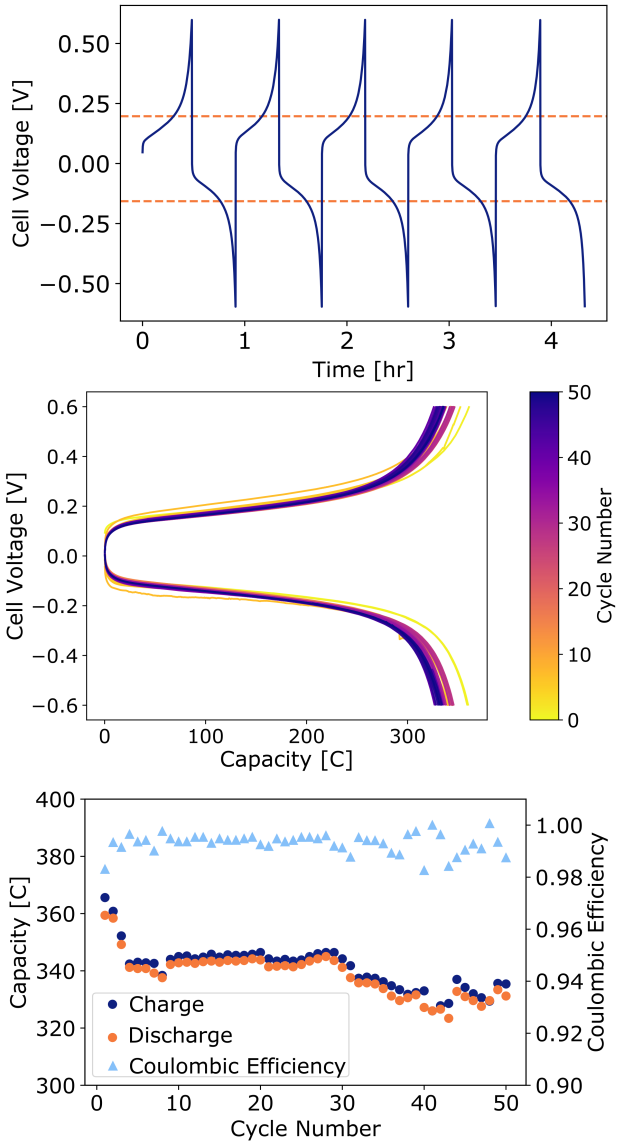

Fig. 3 Compiled figures of merit for the RFB cell containing $Fe^{3+/2+}$ electrolyte in an unbalanced, compositionally symmetric configuration: (a) cell voltage vs. time during a 5-cycle charge–discharge experiment at ±20 mA/cm^2; (b) cell voltage vs. capacity data compiled over a longer 50-cycle charge–discharge experiment; (c) capacity and coulombic efficiency versus cycle number for the same 50-cycle experiment shown in (b).

potential (E_{oc}) from the UME voltammetry data as the applied potential vs. Ag/AgCl when the current density traversed through 0 mA/cm^2 during each CV sweep. These values are plotted in Panel 4b using the righthand y-axis alongside cell voltage on the lefthand y-axis. These data are directly indicative of the state of charge (SOC) of the capacity limiting electrolyte through the Nernst equation:

$$E_{oc} = E^{0\prime} - \frac{RT}{nF} \ln \frac{[Fe^{2+}]}{[Fe^{3+}]} \quad (1)$$

where

$$SOC = \frac{[Fe^{3+}]}{[Fe^{3+}] + [Fe^{2+}]} \quad (2)$$

and all symbols have their regular electrochemical definitions.[42] These data provide similar information to the open-circuit potential excursions used in galvanostatic intermittent titration technique (GITT) measurements,[87,88] with the added benefit that the charge–discharge experiment need not be interrupted. Note, however, that reliable E_{oc} data can only be collected using UMEs with relatively fast electron-transfer rates for the electrolyte of interest (e.g., Pt in this case); otherwise the electrode will pass nearly zero current over a wide range of electrode potentials, yielding ambiguous E_{oc} values. We also observed a distinct time lag between the maximum or minimum SOC implied by E_{oc} values in the analytical cell and the moment at which the RFB changed charge direction. This is broadly consistent with the finite time interval required for electrolyte to flow between the RFB and the analytical cell, and it may also be attributable to nonuniform mixing of the electrolyte as it exits the RFB and enters the analytical cell.

In the measurements shown in Panel 4b, the E_{oc} values varied from 0.377 to 0.443 V vs. Ag/AgCl. The midpoint of this potential range was taken as an empirical estimate of the formal potential $E^{0\prime}$ under the assumption that the capacity limiting electrolyte charges and discharges over SOC values that are symmetric about 50 %. Such an assumption is generally valid as long as the fundamental transport properties of the electrolyte do not change significantly as a function of SOC. This is convenient because temporal changes in the apparent $E^{0\prime}$ over the course of a charge–discharge experiment, or from run to run, could be indicative of electrolyte degradation or drifting of the equilibrium potential in the reference electrode. Indeed, we found that $E^{0\prime}$ varied over the range from 0.32 to 0.57 V vs. Ag/AgCl over 15 experimental runs executed with a single Ag/AgCl reference electrode, but we did not observe significant drift during any single run.

Alongside the ability to visualize and quantify changes in the electrolyte composition, voltammetry measurements in the analytical cell can be used to measure and compare electron-transfer rates across different UME compositions and surface treatments. Panel 4c depicts current density vs. applied potential in the voltage range bracketing the open-circuit potential for Pt and carbon fiber UMEs, where the carbon fiber electrodes were measured before and after surface activation using an electrochemical oxidation procedure that we studied previously on glassy carbon

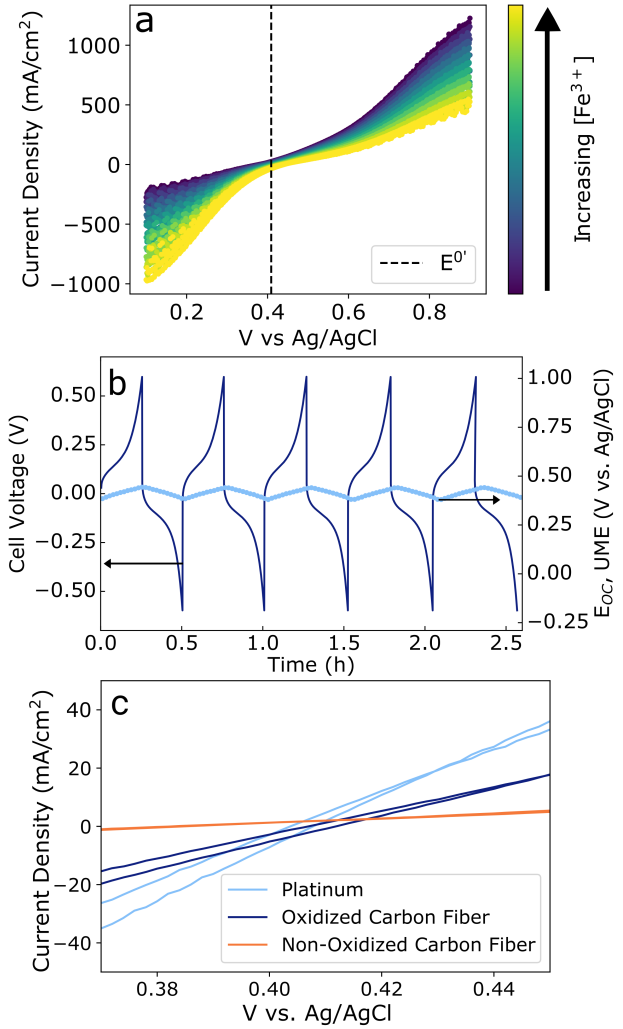

Fig. 4 Compiled data from continuous voltammetric cycling of UMEs in the analytical cell: (a) CV data extracted from the minimum to the maximum state of charge accessed by the RFB; (b) open-circuit potential at a Pt UME (right axis) overlaid against RFB cell voltage (left axis) as a function of time (note that the y axes were scaled so that 0 V cell voltage corresponds to $E^{0\prime}$ in the analytical half cell); (c) current density vs. potential data collected at 50 % state of charge for each of the three electrode types used in this study. All carbon fiber electrodes were first treated in isopropanol that had been pre-purified with activated carbon, and oxidized carbon fiber electrodes were further treated by cycling to highly oxidizing potentials in sulfuric acid solution.

macroelectrodes.[82] These data were extracted from continuous voltammery measurements by selecting the voltammograms that were nearest to $SOC = 50$ %. Despite the modest difference in E_{oc} in these datasets, the slopes of current density vs. potential clearly show that electron transfer rates varied in the order Pt > oxidized carbon fiber > pristine carbon fiber, in qualitative agreement with our prior findings.[81,82]

Quantifying Electron Transfer Rates

We further sought to quantify the differences in electron-transfer kinetics across the three electrode types used in this study. We were specifically interested in devising a general approach to extract k^0_{eff} values from UME voltammetry data that overcomes some of the challenges outlined in the Introduction section and that is amenable to statistical analysis. Figure 5 illustrates the approach we adopted, which we term the shrinking overpotential method, by applying it to voltammetry data that were simulated using finite difference techniques with a commercial software tool called DigiElch.[89]

The approach involves first picking a set of overpotential values, $\pm\eta_1$, at or near the outer bounds of the range of available data and symmetric about the equilibrium formal potential of the redox couple of interest (Panel 5a). We then perform a least-squares regression of these data to the Butler-Volmer equation, which describes current vs. overpotential relationships in the absence of transport and resistive losses.

$$J = nFk^0\left[C_{ox}exp\left(\frac{-\alpha F\eta}{RT}\right) - C_{red}exp\left(\frac{(1-\alpha)F\eta}{RT}\right)\right] \qquad (3)$$

In Panel 5a, the overpotential range between $-\eta_1$ and η_1 extend nearly to the anodic and cathodic limiting current densities J_{lim}. Thus, these data include significant contributions from mass transfer, which results in a systematic under-estimate of k^0_{eff} when fitting to the Butler-Volmer equation.

We then iteratively decrease the overpotential range ($\pm\eta_n$) and reapply the fitting routine, ultimately converging on a fit applied only to the region in the near vicinity of $E^{\circ\prime}$ (Panel 5b; note that an animated version of this panel is included as Electronic Supplementary Information). During this iterative process, the apparent k^0_{eff} value and the goodness-of-fit increases as the overpotential range shrinks to encompass the region that is dominated by kinetic contributions. Ultimately, the k^0_{fit} values converge on a maximum that can be taken as an estimate of the "true" value of k^0_{eff} (Panel 5c). Example data and code to replicate Panel 5c have been archived in a digital repository on Github.[90]

We constrained the charge transfer coefficient, α, in the Butler-Volmer equation to be 0.5 for all the work in this study. In principle, α could be included as an additional unknown to be fit to the Butler-Volmer equation in the regression analysis. However, this is likely to lead to unphysical or widely varying values of α when the fit includes the mass transfer limited regions of a steady-state voltammogram. Thus, if incorporating α into the fit, its value should be still constrained within a relatively narrow range, e.g., from 0.2 to 0.8. Setting a constraint on α in this way is justifiable because very large (near 1) or small (near 0) values of α often reflect a more complex electron-transfer mechanism that is not well described by the Butler-Volmer equation. We also found the systematic error introduced by constraining α to an incorrect value was considerably smaller than the measurement uncertainty that resulted from averaging multiple experimental runs (see Electronic Supplementary Information).

In reality, the maximum value of k^0_{fit} is only a valid estimate of k^0_{eff} if it is smaller than the characteristic mass transfer rate in the analytical cell. When the electron transfer rate approaches or exceeds the rate of mass transfer, the result is a systematic underestimate of k^0_{eff} (Panel 5d) such that the maximum value of k^0_{fit} can only be taken as a lower-bound. Note that this limitation is not specific to our experimental configuration—it is true for any measurement of electron-transfer kinetics based on steady-state voltammetry. Mathematical techniques like Koutecký-Levich analysis can be used to further decrease the impact of mass-transfer limitations, but kinetic analysis depends fundamentally on the ability to measure reaction rates in a kinetically limited regime.[42]

It is possible to estimate a reasonable "upper speed limit" of k^0_{eff} values that can be measured accurately by converting k^0_{eff} to an exchange current density,

$$J_0 = nFk^0_{\text{eff}}\frac{C_{ox}+C_{red}}{2} \qquad (4)$$

which must be smaller than the mass-transfer limited current density J_{lim} to yield a valid estimate of k^0_{eff} . The exact amount that J_0 must be smaller than J_{lim} depends on the amount of error that can be tolerated, but we consider $J_{lim} \geq 3J_0$ to be a reasonable requirement. In the case of the simulated data in Figure 5, $J_{\text{lim}} = 3J_{0,\text{eff}}$ when $k^0_{\text{eff}} = 2\times10^{-3}$ cm/s; hence, k^0_{fit} values diverge from the true value around $k^0_{\text{actual}} = 10^{-3}$ cm/s and above (Panel 5d). Faster k^0_{eff} values can also be measured by simply increasing the rate of mass-transfer in the system. This can be accomplished by further decreasing the size of the UME or by increasing the linear flow rate in the analytical cell. Prior work has shown that mass transfer coefficients on the order of 1 cm/s can be obtained in this way.[91–93]

In addition to the ability to measure relatively high k^0_{eff} values, the shrinking overpotential method has several beneficial features that make it useful for characterizing electron-transfer rates for RFB electrolytes. The first is that it requires only one set of current–overpotential data to estimate k^0_{eff} , and the accuracy of this estimate is not sensitive to varying the battery SOC at least over the range from 10 to 90% (as illustrated in Panels 5c and d). This makes it possible to measure reaction kinetics rapidly and continuously using voltammetry data like those shown in Figure 4. This type of data is easy to collect using in-line flow cell measurements (even without the use of UMEs) or using battery electrodes directly, provided the cell potentials can be converted to overpotentials using a suitable reference. A second key benefit is that this approach does not depend on knowledge of the mass-transfer limited current density, nor does it require that the range of applied potentials extend all the way to the purely mass-transfer limited regime. This makes it possible to extract valid kinetic information even from battery systems in which mass-transfer limited rates cannot be accessed.

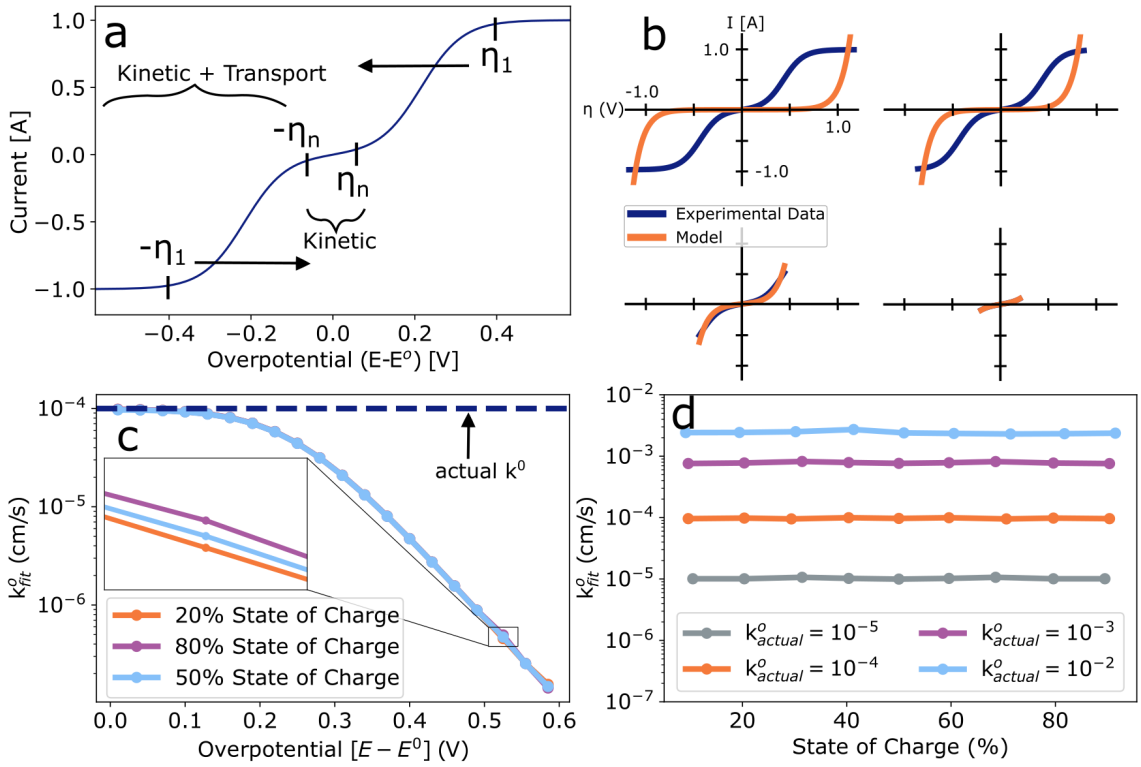

Fig. 5 Empirical workflow for the shrinking overpotential method: (a) iteratively decreasing the range of overpotential values over which a kinetic fit is applied results in a progressive transition from the mixed transport-kinetic regime to the kinetically controlled regime; (b) examples of individual fits to the Butler-Volmer equation as a function of the overpotential range used for the fit; (c) k^0_{fit} vs $|\eta|$ data showing a monotonic increase in the apparent rate constant followed by asymptotic approach to the true value (the inset scales the boxed region to show that all 3 lines nearly overlay); (d) compiled maxima for k^0_{fit} data as in Panel (c) over SOC values ranging from 10 to 90 % and k^0 values from 10^{-5} to 10^{-2} cm/s. Current versus overpotential data used for these fits were generated using finite difference simulations (DigiElch).

In the limit of $\pm\eta_n \to 0$, the shrinking overpotential method is mathematically identical to the polarization resistance method,[42,94,95] which uses a linear approximation of the Butler-Volmer equation to extract electron-transfer rate constants from the region near the equilibrium potential. Indeed, it is not strictly necessary to perform fits over such a wide range of $\pm\eta$ values when the most accurate estimate of k^0_{eff} comes from the region near $\eta = 0$. Nonetheless, the benefit of extending fits to large η values is that no assumptions need to be made about where mass-transfer limitations begin to dominate the J vs. η relationship. Thus, it allows us to empirically identify and use the entire region in a set of voltammetry data over which kinetics dominates the overpotential response. The ability to fit to overpotential ranges extending beyond the region where the linear approximation of the Butler-Volmer equation is no longer valid also reduces the negative impact of background processes like side reactions and capacitance, which can dominate the electrode response at low current.

The shrinking overpotential method also provides a useful mechanism to determine that the reaction rate may be so fast that k^0_{eff} cannot be reliably measured. The hallmark of this behavior is a persistently sloping $|\eta_n|$ vs. k^0_{fit} response with no clear asymptote, as shown in the Electronic Supplementary Information (Figure S3). Moreover, the shrinking overpotential method should be flexible enough to facilitate the use of more complex kinetic models, including those involving multi-step catalytic mechanisms that may not be amenable to linearization in the same way as the Butler-Volmer equation.

Experimental Kinetics Characterization

Finally, we applied the shrinking overpotential method to the voltammetry data we collected in the analytical cell at Pt, carbon fiber, and oxidized carbon fiber UMEs. Figure 6 compiles representative results; complete results are collected in the Electronic Supplementary Information.

Panel 6a depicts representative $|\eta|$ vs. k^0_{fit} data for each electrode type at 50 % SOC from near the beginning of a 5-cycle experimental run. Each dataset yields the expected increase in k^0_{fit} as the overpotential range shrinks. The general trend is also consistent with prior results, where pristine carbon fiber electrodes yielded the slowest electron-transfer rate and Pt electrodes yielded the highest.[81,82] However, these data generally do not yield clear asymptotes in k^0_{fit} at small values of $|\eta|$; we attribute this to the prevalence of background capacitance and electrical noise in the voltammetry measurements, which result in poorer fits and noisier k^0_{fit} results as the fitted overpotential range shrinks to encompass only a few data points. This problem is likely exacerbated by the use of UMEs, which give sub-nA current flow near E_{oc}, making measurements especially sensitive to vibrations and electrical interference.

Panel 6b demonstrates a full set of k^0_{eff} vs. time data for a Pt UME during a 5-cycle charge–discharge experiment, where k^0_{eff} was taken as the maximum value of k^0_{fit} in the shrinking overpotential analysis. These data have been further plotted against SOC, which was extracted from E_{oc} data in the analytical cell. Here an intriguing set of trends emerge, where k^0_{eff} increases and decreases with SOC (i.e., higher concentration of Fe^{3+} yields faster rate and vice-versa) and the overall range of k^0_{eff} values also increases by a factor of 2–3 over several hours. The latter result was consistent across multiple Pt measurements, which leads us to conclude that the Pt surface is modified by Fe^{3+} (e.g., via etching or surface functionalization) in a way that favorably impacts the associated reaction kinetics. Both types of carbon electrode also yielded k^0_{eff} values that varied systematically with SOC, but neither showed persistent changes in k^0_{eff} over time (see Electronic Supplementary Information, Figure S2). Hence, we tentatively conclude that the SOC-dependence of k^0_{eff} is an artifact that also results from the influence of electrical noise and background capacitance on the regression fit. Neither capacitance nor random noise were included in the simulated data in Figure 5, and they might be expected to have a larger impact at more extreme states of charge since the magnitude of the anodic and cathodic current flows are small at high and low SOC, respectively.

Panel 6c compiles k^0_{eff} values extracted from their peaks at the maximum SOC across all 5 charge–discharge runs. Again, we see clear evidence for increasing rate constant, but the relative variation in initial k^0_{eff} is comparable in magnitude to the relative change in rate constant over time. Additional statistical analysis, in which we have estimated upper and lower bounds of k^0_{eff} at a 95 % confidence interval, mainly show an increased spread in the data (albeit asymmetrically biased in the positive direction) as the Pt UMEs were cycled continuously in $Fe^{3+/2+}$. Moreover, these results all fall in the range of $k^0_{\text{eff}} \sim 10^{-3}$ cm/s, which is near the upper bound of what can be accurately measured with $J_{\text{lim}} \sim 1$ A/cm^2. Accordingly, the primary finding agrees with our prior work showing that Pt electrodes catalyze $Fe^{3+/2+}$ redox chemistry very efficiently, and we tentatively conclude that Pt may become further activated upon extended cycling.

Panel 6d compiles the equivalent bounded range of k^0_{eff} values with 95 % confidence intervals across all three electrode types. These data demonstrate that, despite run-to-run variation, we are able to estimate electron-transfer rate constants within a precision of approximately a factor of 3, or half an order of magnitude. These data also clearly show that pristine and oxidized carbon electrodes give stable reaction kinetics over at least 3–4 hours of continuous cycling. Moreover, oxidized carbon fiber UMEs catalyze $Fe^{3+/2+}$ oxidation/reduction 3–4 times more efficiently than pristine carbon fiber UMEs. Indeed, we speculate that k^0_{eff} values of 4–5 $\times 10^{-4}$ cm/s shown by oxidized carbon fiber are fast enough to translate to negligible overpotential losses at operating current densities in the hundreds of mA/cm^2 when combined with the ability to increase roughness factor (electroactive area normalized to superficial area) by 10–100 using porous electrodes derived from carbon fibers.[96]

While the ability to measure interfacial electron transfer rates continuously during RFB operation is useful, extending these types of measurements to technologically relevant electrodes remains a key challenge.[97–102] To this end, it is difficult to extract microscopic reaction rates (e.g., turnover rate per electrochemical surface area) from the types of porous carbon cloth, paper, or felt electrodes that are used in RFBs.[103] Alternatively, if the surface

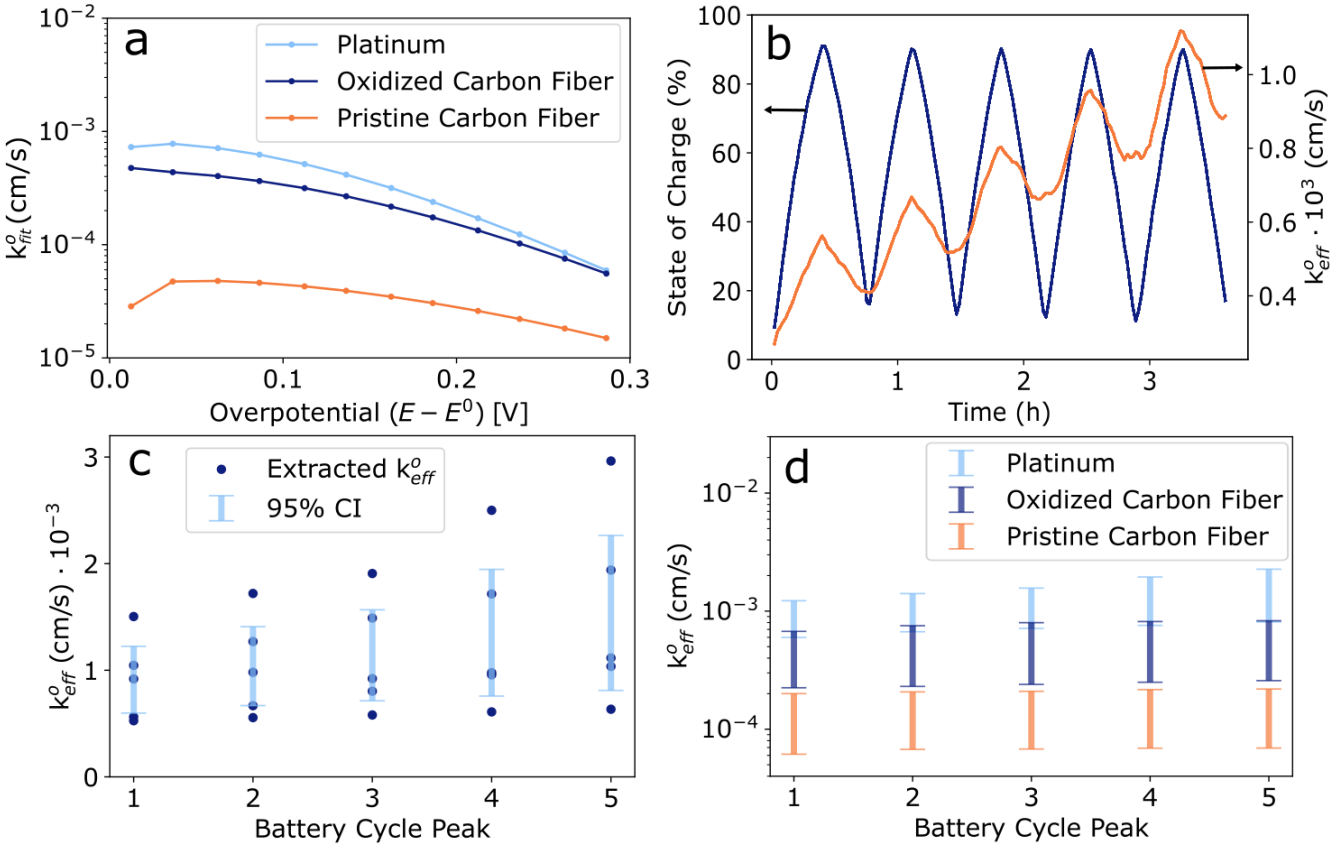

Fig. 6 Empirical kinetics data for three types of UME electrode in $Fe^{3+/2+}$ RFB electrolyte: (a) representative k^0_{fit} vs. $|\eta|$ data for Pt, pristine carbon fiber, and oxidized carbon fiber electrodes extracted from voltammograms near 50 % SOC; (b) k^0_{eff} and SOC vs. time data for a single Pt UME, where k^0_{eff} was taken as the maximum value of k^0_{fit} as depicted in (a); (c) compiled k^0_{eff} values extracted from the battery cycle peaks (points at which the SOC was maximized) for 5 separate experimental runs using a Pt UME, along with statistical estimates of the upper and lower bounds at a 95 % confidence interval; (d) upper and lower bound estimates of k^0_{eff} as in (c) for each of the three electrode types.

.

chemistry of these materials could be replicated in a nonporous, flat electrode configuration, it would be possible to extract k^0_{eff} values for use in kinetic/transport models to predict the overpotential behavior of porous RFB electrodes.[104] Replicating surface chemistry in this way can be accomplished by removing individual carbon fibers from commercial porous carbon electrodes and using them for analytical measurements, as has been demonstrated for aqueous VRFB electrolytes.[72,94,105] It may also be possible to prepare non-porous electrodes on flat substrates using the same types of polymer precursors and thermal treatments as are used to make commercial carbon fibers.[106,107] We see these as among the best ways forward for the development of model RFB electrodes to study the impact of surface chemistry, and the incorporation of additional catalytic units, on electron-transfer kinetics in RFBs over extended operation.

Conclusions

We have described here the construction and operation of a channel-flow UME analytical platform for executing continuous voltammetric measurements inline with the operation of a functional RFB. Operating the battery in an unbalanced, compositionally symmetric configuration enables stable cycling while simultaneously measuring the temporal evolution of electrolyte composition and reaction kinetics in the coupled analytical cell. We have also demonstrated a method for extracting electron transfer rate constants from voltammetry data that overcomes several of the key challenges associated with conventional techniques, particularly the need to make explicit measurements of mass-transfer controlled reaction rates. This approach benefits from very high rates of mass transfer achievable with UMEs, but it should be applicable to other electrode and cell geometries provided there exists a potential region over which the current-overpotential behavior is dominated by kinetics. Rate constants for $Fe^{3+/2+}$ chemistry were found to vary in the order Pt > oxidized C > pristine C, in good agreement with prior work using stationary and rotating-disk electrode voltammetry. Pt electrodes were further found to increase in catalytic activity over at least several hours of cycling in Fe electrolyte, albeit with increasing variability over time.

These results, along with the ability to estimate rate electron transfer rate constants up to ~0.1 cm/s (by increasing electrolyte flow rate) with a precision of approximately half an order of magnitude, make us confident that these approaches will be broadly useful for further applications in RFB materials discovery. Accordingly, this work sets the stage for future studies aimed at tackling several key research questions and outstanding challenges. Chief among these is whether it is possible to develop cost-effective electrode materials in parallel with novel RFB electrolyte chemistries to minimize efficiency losses attribute to electron-transfer kinetics. Studies along these lines will benefit from the ability to make extended measurements directly alongside flow battery operation, but it remains to be seen whether the range of electrode compositions that are accessible in UMEs can accurately replicate the surface chemistry of practical RFB electrodes. Another challenge involves the use of commercial, liquid-filled reference electrodes, which we found to be a weak point due to the tendency for their potentials to drift under extended experimentation in harsh HCl-based electrolytes. Similar challenges are likely to be encountered in many RFB electrolytes, particularly nonaqueous RFBs for which reference electrodes are even less standardized. Extensions toward electrolytes that are oxygen sensitive will also likely require modifications to the experimental apparatus to exclude atmospheric air. These and other challenges are certainly worth tackling in the interest of advancing flow batteries and continuous-flow electroanalytical techniques more broadly.

Author Contributions

B.S. provided formal analysis and drafted the manuscript; Z.P. performed charge-discharge experiments and drafted the manuscript; C.Y. and T.H. performed initial flow cell experiments; T.S., C.Y., and T.H. developed the original flow cell device; T.S. designed and oversaw preliminary studies and compiled prior literature reports of electron-transfer rates; D.M. performed initial simulations; J.M provided funding acquisition and supervision. All authors participated in manuscript review and editing.

Conflicts of interest

B. Segel is in the initial stages of forming a startup company that is developing analytical methods for flow battery materials discovery and design. J. McKone is named as an inventor on two patents covering technologies related to redox flow batteries.

Acknowledgements

This work was supported by a research award from the National Science Foundation Directorate for Engineering (CBET2015859). The authors also acknowledge the University of Pittsburgh and the Mascaro Center for Sustainable Innovation for financial support of the initial phases of this work.

Notes and references

1 L. Li, S. Kim, W. Wang, M. Vijayakumar, Z. Nie, B. Chen, J. Zhang, G. Xia, J. Hu, G. Graff, J. Liu and Z. Yang, *Advanced Energy Materials*, 2011, **1**, 394–400.

2 N. Xu, X. Li, X. Zhao, J. B. Goodenough and K. Huang, *Energy & Environmental Science*, 2011, **4**, 4942–4946.

3 Y. K. Zeng, T. S. Zhao, L. An, X. L. Zhou and L. Wei, *Journal of Power Sources*, 2015, **300**, 438–443.

4 W. Wang, Q. Luo, B. Li, X. Wei, L. Li and Z. Yang, *Advanced Functional Materials*, 2013, **23**, 970–986.

5 L. Trahey, F. R. Brushett, N. P. Balsara, G. Ceder, L. Cheng, Y. M. Chiang, N. T. Hahn, B. J. Ingram, S. D. Minteer, J. S. Moore, K. T. Mueller, L. F. Nazar, K. A. Persson, D. J. Siegel, K. Xu, K. R. Zavadil, V. Srinivasan and G. W. Crabtree, *Proceedings of the National Academy of Sciences of the United States of America*, 2020, **117**, 12550–12557.

6 C. Prochaska and M. Gonzales Harsha, *Energy Storage Grand Challenge: Energy Storage Market Report*, United states department of energy technical report, 2020.

7 A. Anisie and F. Boshell, *Utility-Scale Batteries Innovation Landscape Brief*, International renewable energy agency technical report, 2019.

8 R. M. Darling, K. G. Gallagher, J. A. Kowalski, S. Ha and F. R. Brushett, *Energy & Environmental Science*, 2014, **7**, 3459–3477.

9 M. Li, Z. Rhodes, J. R. Cabrera-Pardo and S. D. Minteer, *Sustainable Energy & Fuels*, 2020, **4**, 4370–4389.

10 P. Alotto, M. Guarnieri and F. Moro, *Renewable and Sustainable Energy Reviews*, 2014, **29**, 325–335.

11 L. H. Thaller and NASA Lewis Research Center, *Intersoc. Energy Conversion Eng. Conf.*, 1974.

12 Y. K. Zeng, X. L. Zhou, L. An, L. Wei and T. S. Zhao, *Journal of Power Sources*, 2016, **324**, 738–744.

13 E. Sum and M. Skyllas-Kazacos, *Journal of Power Sources*, 1985, **15**, 179–190.

14 M. Skyllas-Kazacos, M. Rychick and R. Robins, *All-vanadium redox battery*, 1988.

15 A. Parasuraman, T. M. Lim, C. Menictas and M. Skyllas-Kazacos, *Electrochimica Acta*, 2013, **101**, 27–40.

16 M. Skyllas-Kazacos, L. Cao, M. Kazacos, N. Kausar and A. Mousa, *ChemSusChem*, 2016, **9**, 1521–1543.

17 M. Skyllas-Kazacos, M. H. Chakrabarti, S. A. Hajimolana, F. S. Mjalli and M. Saleem, *Journal of The Electrochemical Society*, 2011, **158**, R55.

18 A. Ciotola, M. Fuss, S. Colombo and W. R. Poganietz, *Journal of Energy Storage*, 2021, **33**, 102094.

19 M. L. Perry and A. Z. Weber, *Journal of The Electrochemical Society*, 2016, **163**, A5064–A5067.

20 L. Su, A. F. Badel, C. Cao, J. J. Hinricher and F. R. Brushett, *Industrial and Engineering Chemistry Research*, 2017, **56**, 9783–9792.

21 F. R. Brushett, M. J. Aziz and K. E. Rodby, *ACS Energy Letters*, 2020, **5**, 879–884.

22 K. Lin, R. Gómez-Bombarelli, E. S. Beh, L. Tong, Q. Chen, A. Valle, A. Aspuru-Guzik, M. J. Aziz and R. G. Gordon, *Nature Energy 2016 1:9*, 2016, **1**, 1–8.

23 D. G. Kwabi, K. Lin, Y. Ji, E. F. Kerr, M. A. Goulet, D. De Porcellinis, D. P. Tabor, D. A. Pollack, A. Aspuru-Guzik, R. G. Gordon and M. J. Aziz, *Joule*, 2018, **2**, 1894–1906.

24 K. Lin, Q. Chen, M. R. Gerhardt, L. Tong, S. B. Kim, L. Eisenach, A. W. Valle, D. Hardee, R. G. Gordon, M. J. Aziz and M. P. Marshak, *Science*, 2015, **349**, 1529–1532.

25 J. Huang, L. Su, J. A. Kowalski, J. L. Barton, M. Ferrandon, A. K. Burrell, F. R. Brushett and L. Zhang, *Journal of Materials Chemistry A*, 2015, **3**, 14971–14976.

26 Q. Liu, A. A. Shinkle, Y. Li, C. W. Monroe, L. T. Thompson and A. E. Sleightholme, *Electrochemistry Communications*, 2010, **12**, 1634–1637.

27 A. E. Sleightholme, A. A. Shinkle, Q. Liu, Y. Li, C. W. Monroe and L. T. Thompson, *Journal of Power Sources*, 2011, **196**, 5742–5745.

28 E. V. Carino, J. Staszak-Jirkovsky, R. S. Assary, L. A. Curtiss, N. M. Markovic and F. R. Brushett, *Chemistry of Materials*, 2016, **28**, 2529–2539.

29 R. W. Hogue and K. E. Toghill, *Current Opinion in Electrochemistry*, 2019, **18**, 37–45.

30 G. Kwon, S. Lee, J. Hwang, H. S. Shim, B. Lee, M. H. Lee, Y. Ko, S. K. Jung, K. Ku, J. Hong and K. Kang, *Joule*, 2018, **2**, 1771–1782.

31 P. Navalpotro, J. Palma, M. Anderson and R. Marcilla, *Angewandte Chemie - International Edition*, 2017, **56**, 12460–12465.

32 M. Pahlevaninezhad, P. Leung, P. Q. Velasco, M. Pahlevani, F. C. Walsh, E. P. Roberts and C. Ponce de León, *Journal of Power Sources*, 2021, **500**, 229942.

33 N. H. Attanayake, J. A. Kowalski, K. V. Greco, M. D. Casselman, J. D. Milshtein, S. J. Chapman, S. R. Parkin, F. R. Brushett and S. A. Odom, *Chemistry of Materials*, 2019, **31**, 4353–4363.

34 S. M. Laramie, J. D. Milshtein, T. M. Breault, F. R. Brushett and L. T. Thompson, *Journal of Power Sources*, 2016, **327**, 681–692.

35 A. Ohira, T. Funaki, E. Ishida, J. D. Kim and Y. Sato, *ACS Applied Energy Materials*, 2020, **3**, 4377–4383.

36 Q. Xu, L. Y. Qin, Y. N. Ji, P. K. Leung, H. N. Su, F. Qiao, W. W. Yang, A. A. Shah and H. M. Li, *Electrochimica Acta*, 2019, **293**, 426–431.

37 N. S. Sinclair, D. Poe, R. F. Savinell, E. J. Maginn and J. S. Wainright, *Journal of The Electrochemical Society*, 2021, **168**, 020527.

38 R. Cheng, J. Xu, J. Zhang, P. Leung, Q. Ma, H. Su, W. Yang and Q. Xu, *Journal of Power Sources*, 2021, **483**, 229200.

39 H. Zhang and C. Sun, *Journal of Power Sources*, 2021, **493**, 229445.

40 Y. A. Gandomi, D. S. Aaron, J. R. Houser, M. C. Daugherty, J. T. Clement, A. M. Pezeshki, T. Y. Ertugrul, D. P. Moseley and M. M. Mench, *Journal of The Electrochemical Society*, 2018, **165**, A970–A1010.

41 D. G. Kwabi, Y. Ji and M. J. Aziz, *Chemical Reviews*, 2020, **120**, 6467–6489.

42 A. J. Bard and L. R. Faulkner, *Electrochemical Methods: Fundamentals and Applications*, John Wiley & Sons, Inc., Danvers, 2nd edn, 2001.

43 R. S. Nicholson, *Analytical Chemistry*, 1965, **37**, 1351–1355.

44 T.-M. Tseng, R.-H. Huang, C.-Y. Huang, K.-L. Hsueh and F.-S. Shieu, *Journal of The Electrochemical Society*, 2013, **160**, A690–A696.

45 E. Martínez-González, H. G. Laguna, M. Sánchez-Castellanos, S. S. Rozenel, V. M. Ugalde-Saldivar and C. Amador-Bedolla, *ACS Applied Energy Materials*, 2020, **3**, 8833–8841.

46 A. Orita, M. G. Verde, M. Sakai and Y. S. Meng, *Nature Communications 2016 7:1*, 2016, **7**, 1–8.

47 H. Wang, S. Y. Sayed, E. J. Luber, B. C. Olsen, S. M. Shirurkar, S. Venkatakrishnan, U. M. Tefashe, A. K. Farquhar, E. S. Smotkin, R. L. McCreery and J. M. Buriak, *ACS Nano*, 2020, **14**, 2575–2584.

48 R. S. Nicholson, *Analytical Chemistry*, 1965.

49 J. Masa, C. Batchelor-McAuley, W. Schuhmann and R. G. Compton, *Nano Research*, 2014, **7**, 71–78.

50 U. A. Paulus, T. J. Schmidt, H. A. Gasteiger and R. J. Behm, *Journal of Electroanalytical Chemistry*, 2001, **495**, 134–145.

51 T. J. Schmidt, H. A. Gasteiger, G. D. Stäb, P. M. Urban, D. M. Kolb and R. J. Behm, *Journal of The Electrochemical Society*, 1998, **145**, 2354–2358.

52 S. N. Pronkin, A. Bonnefont, P. S. Ruvinskiy and E. R. Savinova, *Electrochimica Acta*, 2010, **55**, 3312–3323.

53 E. Siebert, A. Hammouche and M. Kleitz, *Electrochimica Acta*, 1995, **40**, 1741–1753.

54 M. J. Escudero, A. Aguadero, J. A. Alonso and L. Daza, *Journal of Electroanalytical Chemistry*, 2007, **611**, 107–116.

55 X. Wu, H. Xu, L. Lu, H. Zhao, J. Fu, Y. Shen, P. Xu and Y. Dong, *Journal of Power Sources*, 2014, **250**, 274–278.

56 A. Di Blasi, O. Di Blasi, N. Briguglio, A. S. Aricò, D. Sebastián, M. J. Lázaro, G. Monforte and V. Antonucci, *Journal of Power Sources*, 2013, **227**, 15–23.

57 C.-N. Sun, F. M. Delnick, D. S. Aaron, A. B. Papandrew, M. M. Mench and T. A. Zawodzinski, *Journal of The Electrochemical Society*, 2014, **161**, A981–A988.

58 F. Q. Xue, Y. L. Wang, W. H. Wang and X. D. Wang, *Electrochimica Acta*, 2008, **53**, 6636–6642.

59 A. Abbas, S. Abbas, A. Bhattarai, N. M. Latiff, N. Wai, A. N. Phan and T. M. Lim, *Journal of Power Sources*, 2021, **488**, 229411.

60 W. H. Wang and X. D. Wang, *Electrochimica Acta*, 2007, **52**, 6755–6762.

61 Y. Xiang and W. A. Daoud, *Journal of Power Sources*, 2019, **416**, 175–183.

62 A. A. Shinkle, A. E. Sleightholme, L. T. Thompson and C. W. Monroe, *Journal of Applied Electrochemistry*, 2011, **41**, 1191–1199.

63 M. A. Miller, J. S. Wainright and R. F. Savinell, *Journal of The Electrochemical Society*, 2016, **163**, A578–A579.

64 J. A. Kowalski, A. M. Fenton, B. J. Neyhouse and F. R. Brushett, *Journal of The Electrochemical Society*, 2020, **167**, 160513.

65 C. G. Zoski, *Handbook of electrochemistry*, Elsevier, 2007.

66 B. Yang, A. Murali, A. Nirmalchandar, B. Jayathilake, G. K. S. Prakash and S. R. Narayanan, *Journal of The Electrochemical Society*, 2020, **167**, 060520.

67 C. A. McDermott, K. R. Kneten and R. L. McCreery, *Journal of The Electrochemical Society*, 1993, **140**, 2593.

68 M. Štulíková and F. Vydra, *Journal of Electroanalytical Chemistry and Interfacial Electrochemistry*, 1972, **38**, 349–357.

69 B. G. Ateya and L. G. Austin, *Journal of The Electrochemical Society*, 1973, **120**, 1216.

70 E. Hollax and D. S. Cheng, *Carbon*, 1985, **23**, 655–664.

71 G. Oriji, Y. Katayama and T. Miura, *Journal of Power Sources*, 2005, **139**, 321–324.

72 A. Bourke, M. A. Miller, R. P. Lynch, X. Gao, J. Landon, J. S. Wainright, R. F. Savinell and D. N. Buckley, *Journal of The Electrochemical Society*, 2016, **163**, A5097–A5105.

73 H. Liu, L. Yang, Q. Xu and C. Yan, *RSC Advances*, 2014, **4**, 55666–55670.

74 Y. Li, J. Parrondo, S. Sankarasubramanian and V. Ramani, *Journal of Physical Chemistry C*, 2019, **123**, 6370–6378.

75 E. Agar, C. R. Dennison, K. W. Knehr and E. C. Kumbur, *Journal of Power Sources*, 2013, **225**, 89–94.

76 X. W. Wu, T. Yamamura, S. Ohta, Q. X. Zhang, F. C. Lv, C. M. Liu, K. Shirasaki, I. Satoh, T. Shikama, D. Lu and S. Q. Liu, *Journal of Applied Electrochemistry*, 2011, **41**, 1183–1190.

77 J. Friedl and U. Stimming, *Electrochimica Acta*, 2017, **227**, 235–245.

78 T. Yamamura, N. Watanabe, T. Yano and Y. Shiokawa, *Journal of The Electrochemical Society*, 2005, **152**, A830.

79 B. Huskinson, M. P. Marshak, C. Suh, S. Er, M. R. Gerhardt, C. J. Galvin, X. Chen, A. Aspuru-Guzik, R. G. Gordon and M. J. Aziz, *Nature*, 2014, **505**, 195–198.

80 A. W. Lantz, S. A. Shavalier, W. Schroeder and P. G. Rasmussen, *ACS Applied Energy Materials*, 2019, **2**, 7893–7902.

81 T. V. Sawant and J. R. Mckone, *ACS Applied Energy Materials*, 2018, **1**, 4743–4753.

82 T. V. Sawant and J. R. McKone, *Journal of Physical Chemistry C*, 2019, **123**, 144–152.

83 M.-A. Goulet and M. J. Aziz, *Journal of The Electrochemical Society*, 2018, **165**, A1466–A1477.

84 Z. Li, L. Liu, Y. Zhao, J. Xi, Z. Wu and X. Qiu, *Journal of Power Sources*, 2019, **438**, 226990.

85 S. Rudolph, U. Schröder and I. M. Bayanov, *Journal of Electroanalytical Chemistry*, 2013, **703**, 29–37.

86 N. H. Choi, S.-k. Kwon and H. Kim, *Journal of The Electrochemical Society*, 2013, **160**, A973–A979.

87 K. W. Knehr, S. Biswas and D. A. Steingart, *Journal of The Electrochemical Society*, 2017, **164**, A3101–A3108.

88 Q. Huang, J. Yang, C. B. Ng, C. Jia and Q. Wang, *Energy & Environmental Science*, 2016, **9**, 917–921.

89 J. D. Hofmann and D. Schröder, *Chemie Ingenieur Technik*, 2019, **91**, 786–794.

90 B. Segel, *Shrinking-Overpotential-Method*, 2022, `https://github.com/bsegel/Shrinking-Overpotential-Method`.

91 J. V. Macpherson, S. Marcar and P. R. Unwin, *Analytical Chemistry*, 1994, **66**, 2175–2179.

92 N. V. Rees, J. A. Alden, R. A. W. Dryfe, B. A. Coles and R. G. Compton, *J. Phys. Chem*, 1995, **99**, 14813–14818.

93 N. V. Rees, R. A. W. Dryfe, J. A. Cooper, B. A. Coles, R. G. Compton, S. G. Davies and T. D. Mccarthy, *J. Phys. Chem*, 1995, **99**, 7096–7101.

94 M. A. Miller, A. Bourke, N. Quill, J. S. Wainright, R. P. Lynch, D. N. Buckley and R. F. Savinell, *Journal of The Electrochemical Society*, 2016, **163**, A2095–A2102.

95 D. Aaron, C. N. Sun, M. Bright, A. B. Papandrew, M. M. Mench and T. A. Zawodzinski, *ECS Electrochemistry Letters*, 2013, **2**, A29.

96 T. V. Sawant, C. S. Yim, T. J. Henry, D. M. Miller and J. R. McKone, *Joule*, 2021, **5**, 360–378.

97 Y. Li, S. Yang, Y. Zhao, N. Mubarak, M. Xu, M. Ihsan-Ul-Haq, T. Zhao, Q. Chen and J.-K. Kim, *Journal of Materials Chemistry A*, 2022, **10**, 5605–5613.

98 I. Mustafa, R. Susantyoko, C. H. Wu, F. Ahmed, R. Hashaikeh, F. Almarzooqi and S. Almheiri, *Scientific Reports 2019 9:1*, 2019, **9**, 1–14.

99 R. Banerjee, N. Bevilacqua, A. Mohseninia, B. Wiedemann, F. Wilhelm, J. Scholta and R. Zeis, *Journal of Energy Storage*, 2019, **26**, 100997.

100 M. Schnucklake, L. Kaßner, M. Mehring and C. Roth, *RSC Advances*, 2020, **10**, 41926–41935.

101 M. Schnucklake, S. Kuecken, A. Fetyan, J. Schmidt, A. Thomas and C. Roth, *Journal of Materials Chemistry A*, 2017, **5**, 25193–25199.

102 A. Forner-Cuenca and F. R. Brushett, *Current Opinion in Electrochemistry*, 2019, **18**, 113–122.

103 S. Yang, Y. Li and Q. Chen, *Journal of Materials Chemistry A*, 2021, **9**, 14025–14031.

104 D. Zhang, A. Forner-Cuenca, O. O. Taiwo, V. Yufit, F. R. Brushett, N. P. Brandon, S. Gu and Q. Cai, *Journal of Power Sources*, 2020, **447**, 227249.

105 A. Bourke, M. A. Miller, R. P. Lynch, J. S. Wainright, R. F. Savinell and D. N. Buckley, *Journal of The Electrochemical Society*, 2015, **162**, A1547–A1555.

106 C. L. Renschler, A. P. Sylwester and L. V. Salgado, *Journal of Materials Research*, 1989, **4**, 452–457.

107 M. Inagaki, S. Harada, T. Sato, T. Nakajima, Y. Horino and K. Morita, *Carbon*, 1989, **27**, 253–257.